Climate-driven shifts in kelp forest composition reduce carbon sequestration potential

Luka Wright (luka@wright.it)
University of Plymouth https://orcid.org/0000-0002-1273-6256

Albert Pessarrodona
University of Western Australia https://orcid.org/0000-0002-6057-9937

Andy Foggo
Marine Biology and Ecology Research Centre, School of Marine Science and Enginieering, University of Plymouth https://orcid.org/0000-0002-0280-0824

Article

Keywords: blue carbon sinks, decomposition, detrital photosynthetic apparatus

Posted Date: October 11th, 2021

DOI: https://doi.org/10.21203/rs.3.rs-957301/v1

Climate-driven shifts in kelp forest composition reduce carbon sequestration potential

Luka Seamus Wright[1,2] * (0000-0002-1273-6256), Albert Pessarrodona[3] (0000-0002-6057-9937) and Andy Foggo[1] (0000-0002-0280-0824)

[1]Marine Biology and Ecology Research Centre, University of Plymouth, Drake Circus, Plymouth, PL4 8AA, United Kingdom.
[2]Queen's University Marine Laboratory, The Strand, Portaferry, BT22 1PF, United Kingdom.
[3]UWA Oceans Institute, University of Western Australia, Crawley, 6009, Australia.

*corresponding author: luka@wright.it

Abstract

The potential contribution of kelp to blue carbon sinks is currently of great interest. In the Northeast Atlantic, kelp forest composition is changing due to climate-driven poleward range shifts of cold temperate *Laminaria digitata* and *L. hyperborea* and warm temperate *L. ochroleuca*. To understand how this might affect carbon sequestration potential, we quantified interspecific differences in carbon export and decomposition alongside changes in detrital photophysiology and biochemistry. We found that warm temperate kelp decomposes up to 155% faster than its boreal congeners, likely due to lower carbon and polyphenolic content. Faster decomposition further causes its detrital photosynthetic apparatus to be overwhelmed after 20 d and lose integrity after 36 d, while cold temperate species maintain carbon assimilation. Besides climate-driven phase shifts, heatwaves, forest miniaturisation, decompositional acceleration and coastal darkening, compositional change such as the predicted dominance of *L. ochroleuca* will likely reduce the carbon sequestration potential of these temperate forests.

Introduction

Over the last decade humans have emitted around 11 billion tons of carbon per year[1]. In the Paris Agreement, 191 countries pledged to reduce this emission and enhance carbon sink capacity. Ocean-based biological carbon dioxide removal (CDR) is now acknowledged as an integral part of fulfilling this goal[1]. Such CDR is facilitated by marine macrophytes, whose role in carbon sequestration was first recognised four decades ago[2] but has only recently come to mainstream attention as blue carbon[1]. Despite the involvement of marine vegetated habitats in CDR and their location within national jurisdiction, few ocean-based nationally determined contributions (NDCs) have been put forward by affluent Annex I parties such as the UK, US and Australia[3] which hold some of the highest blue carbon wealth[4]. In part, this may be due to the ongoing debate on the blue carbon status of temperate kelp forests that dominate the coasts of these countries[5]. Therefore, identifying the magnitude and fate of carbon assimilated by these marine plants is key to our understanding of their carbon sequestration potential (CSP) and their consequent inclusion in blue carbon frameworks[5].

CSP is a function of carbon export and fate[6,7] and can be defined as the decline in carbon available for sequestration after export. Carbon export is determined by the magnitude of exported biomass and tissue carbon content[7–10], while variance in carbon fate is attributable to differential remineralisation. The two processes that constitute remineralisation are consumption by detritivores and degradation by microbial saprotrophs[6,7], hereafter collectively referred to as decomposition. Marine plants that have higher carbon-nutrient ratios or carbon content[11,12], slower growth[13], more refractory compounds[14] and more polyphenols[15] decompose more slowly. Therefore, macroalgae generally decompose slower than phytoplankton and faster than seagrasses[6], endowing them with an intermediate relative CSP (Fig. 1b). Nonetheless, they are globally more abundant than seagrasses[16]. Hence their absolute CSP[17] is thought to be 158% greater than that of seagrasses and only 25% smaller than that of phytoplankton (Fig. 1a). Although this estimate[17] is widely taken at face value, the truth is that uncertainty surrounding macroalgal carbon sequestration remains substantial[18].

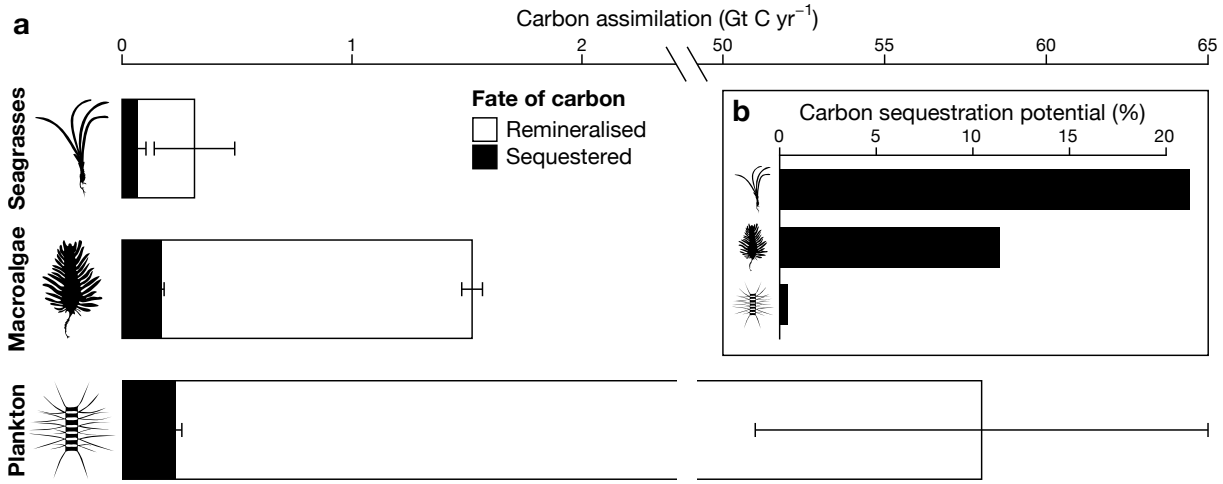

Figure 1. Estimated magnitude and fate of marine autotrophic production. **a**, Global marine net carbon assimilation and putative sequestration of seagrasses, macroalgae and phytoplankton. A proportion of production is sequestered (black), while the majority is remineralised (white). **b**, Percentage of production that is sequestered. Bars and error bars indicate estimated means and putative confidence intervals. For macro- and microalgae these are 95% confidence intervals, while error bars for seagrasses represent half range uncertainty (Table S1).

Variance in carbon export, decomposition and burial is recognised to bring about large interspecific differences in the CSP of seagrasses[7,19] and mangroves[20,21]. However, a similar interspecific comparison is lacking for macroalgae, despite two additional major sources of variability in this group: detrital floating time and transport distance range from a few seconds[22] and metres[23] to thousands of hours[24] and kilometres[25]. Therefore, data scarcity on interspecific diversity must certainly lead to errors in estimates of global CSP[19]. For instance, the latest CSP estimate for macroalgae[17] was calculated using only between one and 20 distinct genera for each parameter with carbon burial based solely on data for *Gracilaria* (Table S2) and reports deceptively small confidence intervals (Fig. 1a). Consequently, this model has been trusted to such an extent that it was recently used to make broad conclusions about the regional and global CSP of *Ecklonia radiata*[26], a species not accounted for in the original estimate (Table S2). We argue that, especially in local and regional contexts, such broad estimates (Fig. 1) are potentially misleading and should be used with caution.

Here we show that interspecific differences in CSP within a single macroalgal genus are large, using kelp forests in the southern UK as a model system (Fig. 2a). These forests have experienced rapid, climate-driven range shifts in species composition over the last century, with increased dominance of a warm temperate kelp[8,27,28] and further changes expected in the near future (Fig. 2a). Additionally, our study location is the only locality worldwide where macroalgal carbon burial in coastal sediments has been empirically documented *in situ*[18]. We first outline differences in carbon export and decomposition speed of *Laminaria* species and investigate potential mechanistic drivers. Based on these parameters we then estimate how CSP differs between species and thus relates to kelp forest composition. The additional dimension of biogeographic shifts and subsequent compositional change gave us the opportunity to also model the effect of ocean warming on the densities of kelps with different thermal tolerances (Fig. 2b), based on historical and future (RCP2.6, RCP6.0 and RCP8.5) sea surface temperature. We finally explore the photophysiology and biochemistry of decomposing detritus to gain further insights into potential feedback loops.

Differential carbon export and decomposition speed

Northeast Atlantic temperate marine forests are mostly dominated by three species of the genus *Laminaria*[29]. Based on their distribution (Fig. 2a) and underlying thermal tolerances (Fig. 2b), two of these species are classed as cold temperate (*L. digitata* and *L. hyperborea*) and one as warm temperate (*L. ochroleuca*)[29]. Our study site within the latitudinal range overlap (Fig. 2a) is currently dominated by the two boreal species, with *L. ochroleuca* occupying 22% of the forest on an annual basis (Table S5). However, at the plant level, *L. ochroleuca* exports 35–71% more carbon per year via distal frond erosion (Table S5), the main mechanism of carbon export beside dislodgement[9,10] and dissolved carbon exudation[30,31].

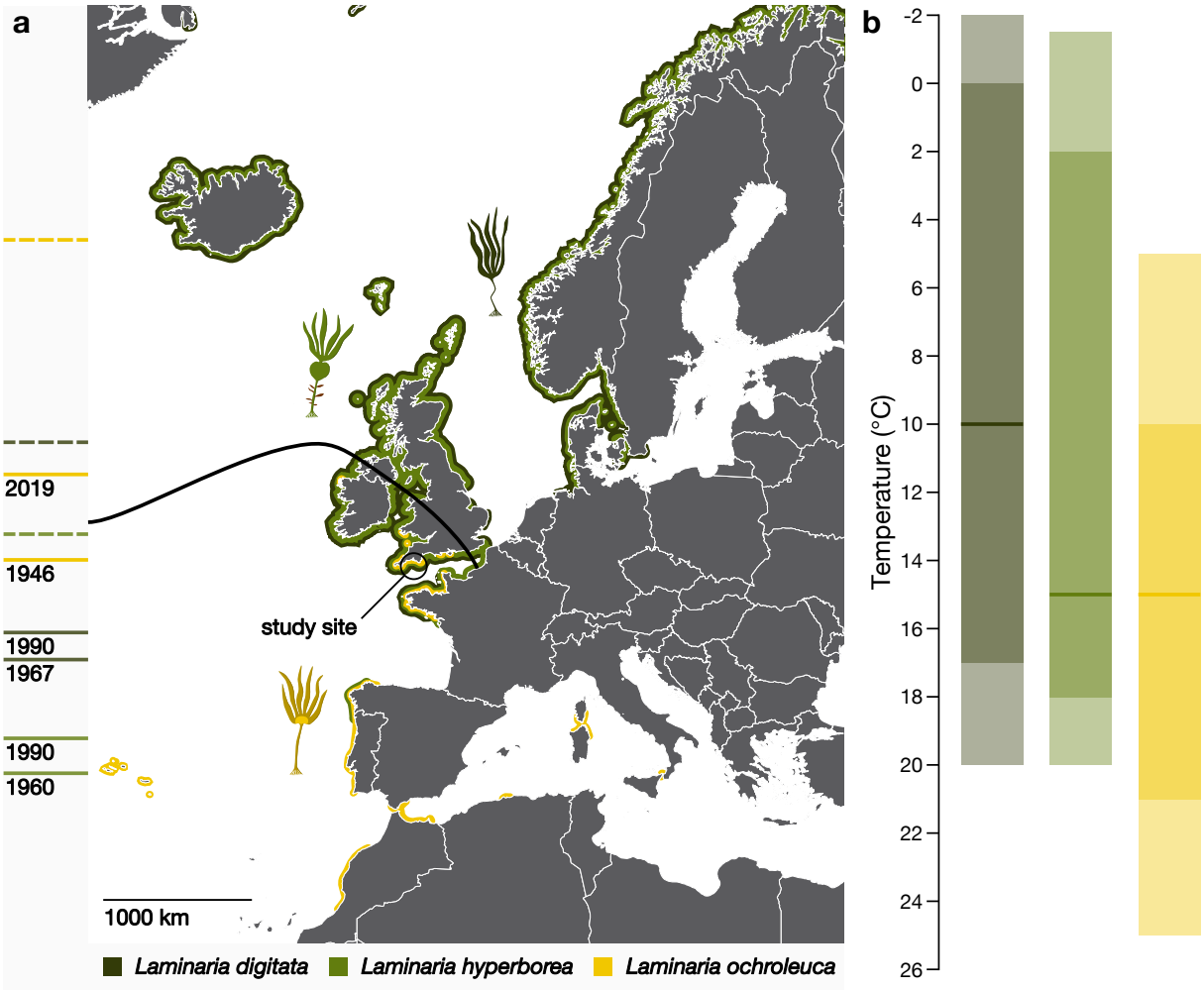

Figure 2. Biogeography of Northeast Atlantic *Laminaria* species. **a**, Current approximate species distributions are shown as coloured coastlines. Past and future (SRES A2 and RCP8.5) trailing (*L. digitata* and *L. hyperborea*) or leading (*L. ochroleuca*) range edges are indicated by solid and dashed lines, respectively (Table S3). Kelp icons denote approximate range centres. The black line indicates the northern biogeographic boundary of warm temperate kelps (Table S3). **b**, Underlying these species distributions are the species-specific temperature optima (lines) and tolerances (shaded areas) of sporophyte growth (light) and gametophyte fertility (dark) (Table S4).

Our findings suggest that areal carbon export is currently highest for *L. hyperborea* (mean ± s.e.m., 211 ± 27 g C m^{-2} yr^{-1}), intermediate for *L. ochroleuca* (127 ± 22 g C m^{-2} yr^{-1}) and lowest for *L. digitata* (90 ± 10 g C m^{-2} yr^{-1}). Importantly, plant standing stock and carbon export also vary seasonally by up to two orders of magnitude (Table S5), with a species-specific pattern evident throughout the year (Fig. S1). Carbon export peaks in spring for *L. hyperborea*, summer for *L. ochroleuca* and autumn for *L. digitata* (Fig. S1, Table S5). The mechanisms underlying these seasonal differences revolve around contrasting growth and senescence strategies and have been adequately discussed for all three species[8,32].

In addition to the outlined interspecific differences in carbon export, the lability of detritus varies considerably between species. In two independetly conducted field experiments we found that *in situ* decomposition occurs 66–155% faster in *L. ochroleuca* than its boreal congeners (Fig. 3a, Table S6, S7). These data are supported by image analysis, which revealed that *L. ochroleuca* had 7.73–18.77 times larger excavation scars (Fig. 3b) and 1.45–4.51 times larger perforation scars (Fig. 3c) caused by grazing over one month on the forest floor (Table S6). The feeding preference of the key detritivores[33] *Steromphala cineraria* and *Patella pellucida*[8,27,34] for *L. ochroleuca* further supports our findings. We also found that kelp detritus decomposes at a 68% higher rate on the forest floor than on adjacent sediment (Fig. 3a, Table S6), which is likely due to the greater abundance of the mentioned macroherbivores within compared to adjacent to the kelp forest.

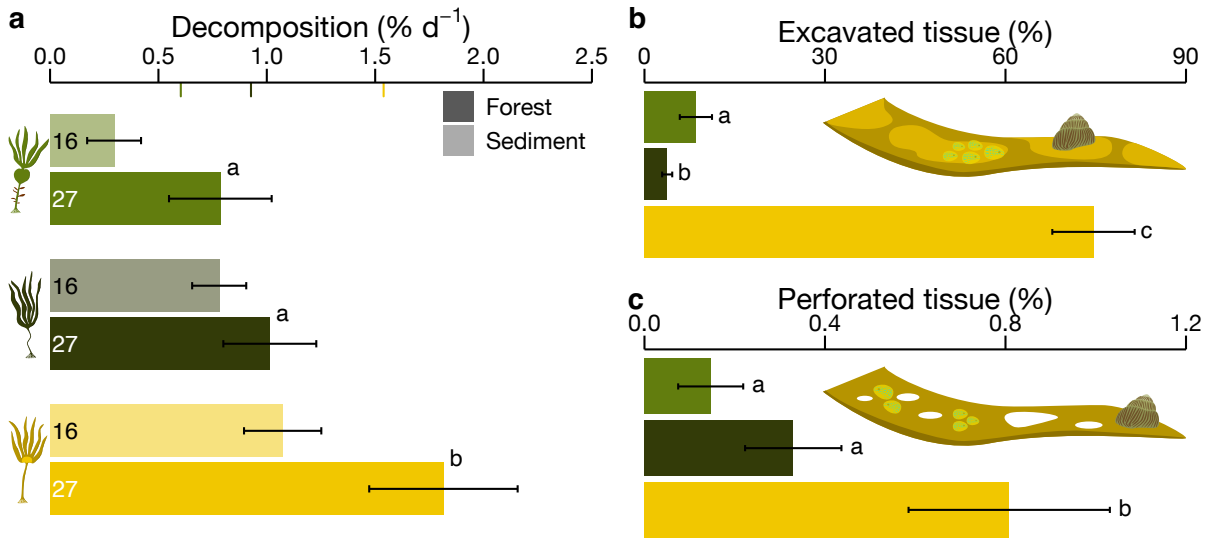

Figure 3. *In situ* decomposition of Northeast Atlantic *Laminaria* species. **a**, Decomposition speed is higher in warm temperate than cold temperate species and on the kelp forest floor than on sediment. Bars and error bars are means ± s.e.m. Coloured axis ticks are overall means for each species. Numbers are sample sizes. Letters indicate groupings of similarity at the 95% confidence level. **b**–**c**, Differential macrodetritivore grazing activity as evidenced by excavation (**b**) and perforation (**c**) scars after 32 d on the kelp forest floor. Bars and error bars are means ± s.e.m. (n = 18). Letters indicate groupings of similarity at the 95% confidence level.

Once these differences in decomposition speed were established, we explored whether interspecific biochemical variation was sufficient to explain them. Indeed, we found that cold temperate species have 27–30% higher carbon content than *L. ochroleuca* and every one percent increase in carbon content decreases the daily decomposition rate by 0.17% (Fig. 4a, Table S6). A similar negative relationship (0.06% d^{-1} %$^{-1}$) was recently reported for *L. hyperborea* and *Saccharina latissima* detritus[12]. Elemental stoichiometry therefore seems to be an important driver of kelp decomposition, which is in line with evidence from various other plants[11].

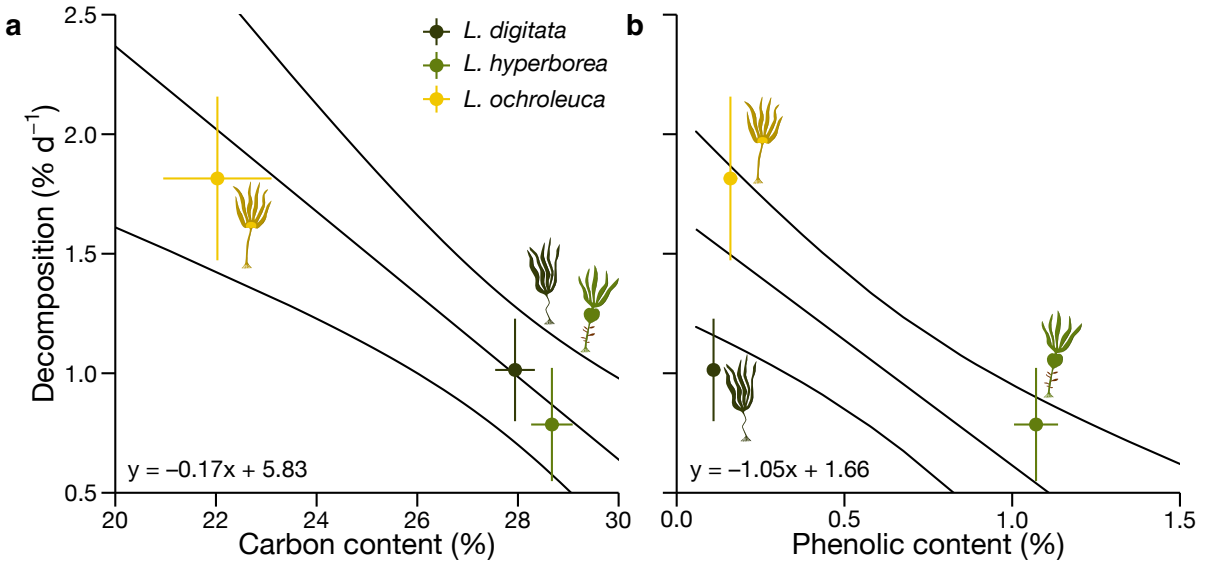

Figure 4. Mechanistic drivers of the differential decomposition speed observed in Northeast Atlantic *Laminaria* species. Interspecific differences in carbon (**a**) and phenolic (**b**) content complement each other to explain the observed discrepancy in decomposition rates in the West Hoe kelp forest. Point ranges are means ± s.e.m. (n = 27). Lines are model predictions and 95% confidence intervals. Intraspecific relationships between phenolic content and decomposition rate are visualised in Fig. S2.

Polyphenols are also known to deter feeding by some herbivores[15] but the story is less clear cut for these chemical defence compounds. While we did find an overall decrease of 1.05% in decomposition speed with every percent increase in soluble phenolic content (Fig. 4b, Table S6), *L. digitata* had a lower concentration than we expected given its low decomposition rate. The low

polyphenol levels in *L. digitata* (cf. ref.[32]) may be compensated by its reactive oxygen species and iodine defence[35], since iodine plays a crucial role in structuring the saprotrophic community in the early stages of decomposition[36]. Intraspecific variation in phenolic content also influences decomposition in *L. hyperborea* (–2.44% d^{-1} $\%^{-1}$) and *L. ochroleuca* (–9.23% d^{-1} $\%^{-1}$) (Fig. S2). Other mechanisms likely include the slower annual growth rate of boreal kelps[8], which negatively correlates with decomposition rate across plant groups[13], alongside differences in tissue toughness (L.S. Wright, personal observation), which may deter grazers.

Carbon sequestration potential

Climate change is reducing the extent of many temperate kelp forests[37]. On top of this general pattern, the CSP of these forests is expected to be diminished by climate-driven phase shifts[38,39], heatwaves[40], forest miniaturisation[9,41], decompositional acceleration[12] and coastal darkening[31]. On the basis of the presented empirical evidence, we suggest that compositional change of these marine forests via climate-driven poleward range shifts is a key mechanism that may further reduce CSP.

Carbon export and decomposition together determine a plant's CSP[6,7]. We therefore estimated linear relationships between current species-specific CSP (g C m^{-2} yr^{-1}) and detrital age (methods section 2.1). As expected, the CSP of *L. cohroleuca* declines 54–135% faster per day than that of the cold temperate species (Fig. 5a). Consequentially, *L. digitata* and *L. hyperborea* CSP reaches zero after 109 ± 12 d and 167 ± 22 d, on average 43 d and 101 d later than that of their warm temperate congener (66 ± 11 d) (Fig. 5a). Interestingly, this contrast is maintained throughout the year despite strong seasonal variation in carbon export: all carbon exported by *L. ochroleuca* is remineralised 52–134 d, 34–74 d, 38–85 d and 54–137 d earlier than that of its boreal congeners in spring, summer, autumn and winter respectively (Fig. S3a).

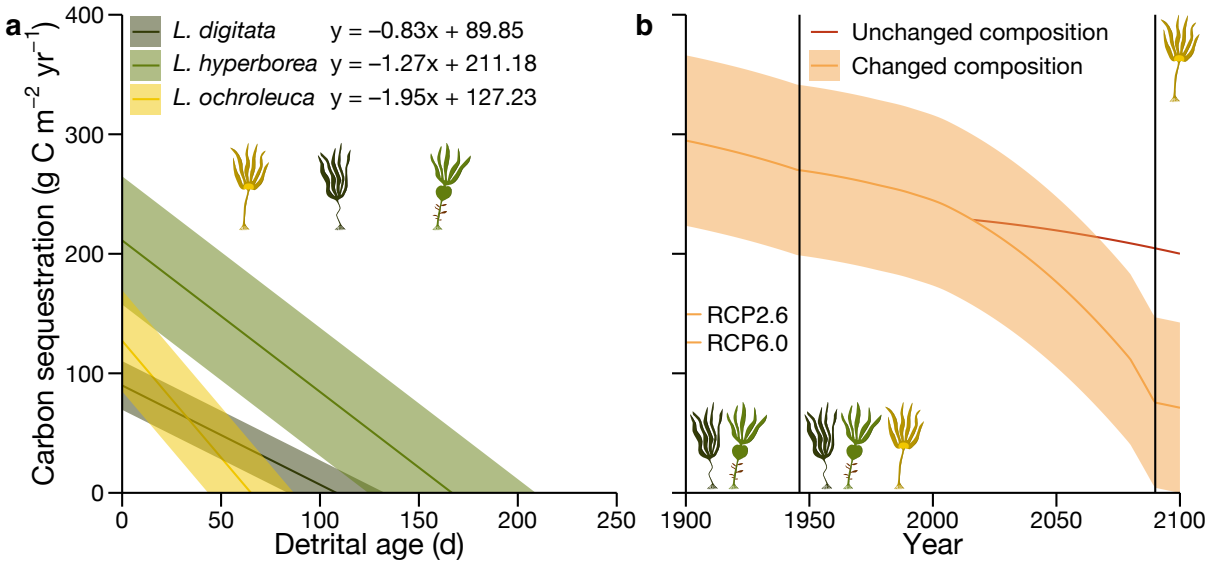

Figure 5. Carbon sequestration potential (CSP) of Northeast Atlantic *Laminaria* species. **a**, Present CSP with increasing detrital age. Lines and shaded areas are estimates and 95% confidence intervals. Kelp icons indicate when CSP reaches zero. **b**, Temporal trend of overall kelp forest CSP over two centuries according to historical sea surface temperature data and RCP8.5 sea surface temperature predictions for the Plymouth Sound region (Fig. S4). Coloured y axis ticks indicate end-of-century CSP according to alternative scenarios (RCP2.6 and RCP6.0 are shown in full in Figure S5). Without a change in forest composition (red line), CSP would only decline slightly due to the enhancing effect of temperature on decomposition speed[12]. All carbon remaining after 50 d (cf. **a**) is assumed to count towards CSP because all species contribute at that detrital age. Lines and shaded areas are estimates and 95% confidence intervals (orange and red confidence intervals are identical and the latter was removed for clarity). Kelp icons and vertical lines indicate stages of compositional change from before the arrival of *L. ochroleuca* in Plymouth Sound in 1946[28] to the predicted local extinction of the cold temperate species in 2090 (cf. Fig. 2).

Climate change is shifting the outlined species distributions (Fig. 2a), based on differential temperature tolerance (Fig. 2b), which is leading to a restructuring of Northeast Atlantic kelp forest composition[8,27,28]. Therefore we modelled the effects of this climate-driven ecosystem alteration on forest carbon export and CSP through time, on the basis of species-specific temperature tolerances,

historical temperature data and representative concentration pathway (RCP) temperature predictions for the region (methods section 2.2, Fig. S4). The purpose of this thought experiment is to highlight interspecific diversity and should therefore be inclusive of all species, regardless of unknown true carbon sequestration. We therefore assume that all carbon remaining after 50 d, when none of the species' exported carbon has fully decomposed (Fig. 5a), constitutes CSP. Our estimates suggest that despite fluctuating but stable carbon export across both centuries (Fig. S5), forest CSP declined by around 0.19% per year in the past and will likely continue to do so at a 3.22 times higher rate (0.82% yr^{-1}) under RCP8.5 (Fig. 5b). RCP6.0 and RCP2.6 are prediced to reduce present CSP 34% and 49% less by the end of the century (Fig. 5b, Fig. S6), which suggests that climate change mitigation may alleviate forest CSP loss. We also accounted for decompositional acceleration due to ocean warming[12] and show that models based solely on this factor[12] underestimate CSP decline across RCPs (Fig. 5b, Fig. S6). Hence, we predict that through a vicious circle, climate-driven range shifts may lead to a reduction of a climate change mitigating ecosystem service.

The modelled interspecific contrasts in CSP are likely underestimates. First, in stark contrast to *L. hyperborea*[27] and *L. digitata* (L.S. Wright, personal observation), *L. ochroleuca* is almost completely devoid of epiphytes (mostly *Palmaria palmata*), which further reduces the carbon load and hence CSP of this species. Second, *L. hyperborea* is unique in shedding over 60% of its laminar biomass, termed the May cast, in spring[8–10] (Fig. S1), which has been suggested to temporarily overwhelm consumers, thus increasing CSP[10]. Third, temperatures are approximately 7°C warmer during peak carbon export by *L. ochroleuca* than *L. hyperborea* (Fig. S1, S4), which corresponds to an increase in decomposition rate of 0.37% d^{-1} in absolute terms and 73% in relative terms[12]. Fourth, *L. hyperborea* detritus remains intact for at least six months on shallow sediment due to exponential decay[36], so our linear model almost certainly overestimates this species' long-term decomposition speed. Finally, export to hypoxic regions of the deep sea has been shown to increase the detrital longevity of this species[42].

Detrital carbon assimilation and potential feedback loops

Kelp detritus can remain photosynthetically active for months *in situ* after being exported[36], sometimes even increasing in mass[36,42]. These findings suggest that macroalgal detritus travelling through illuminated zones can resist carbon loss, although laboratory experiments have shown that responses differ between species[43]. We present the first interspecfic comparsion of detrital photophysiological viability *in situ* and found that *L. digitata* and *L. hyperborea* maintained net primary production at 0.98 and 0.76 mg C g^{-1} h^{-1} over one month on the forest floor (Fig. 6a). In contrast, photosynthesis of *L. ochroleuca*, which was initially 48–50% lower than that of its cold temperate congeners, declined at a rate of 0.03 mg C g^{-1} h^{-1} per day (Fig. 6a). Consequently, *L. ochroleuca* was emitting carbon after 20 d and assimilating 1.43 and 1.14 mg C g^{-1} h^{-1} less than *L. digitata* and *L. hyperborea* after one month. Gross primary production displayed a similar pattern (Fig. S7), indicating that increased microbial respiration[36] is not the primary driver and the photosynthetic apparatus of *L. ochroleuca* is in fact failing after 36 d of decomposition. The lower photosynthetic activity of *L. ochroleuca* may be attributable to its 42–45% lower total photosynthetic pigment concentration[44].

These results have major implications for detrital carbon assimilation in different photoenvironments which in turn affects decomposition. Using regional photon flux density data and photosynthesis-irradiance relationships (method section 2.3), we estimate that cold and warm temperate species can increase their respective yearly carbon export by 53–87% and 4% via detrital carbon assimilation. On an annual basis, boreal kelps can potentially assimilate 5–199% more carbon during their detrital phase than *L. ochroleuca*. Interestingly, cold temperate species have higher cumulative carbon assimilation throughout the year except for summer, when *L. ochroleuca* detritus could potentially assimilate 1.95–4.52 times more carbon on its way to local sinks[18] (Fig. S3b). Across species, carbon assimilation generally declines from spring through to winter rather than peaking in summer as expected from seasonal light availability (Fig. S3b). Depending on the light regime, disintegration of the photosynthetic apparatus of *L. ochroleuca* due to decomposition is a significant positive feedback loop that may further exacerbate interspecific differences in CSP beyond those reported above (Fig. 5).

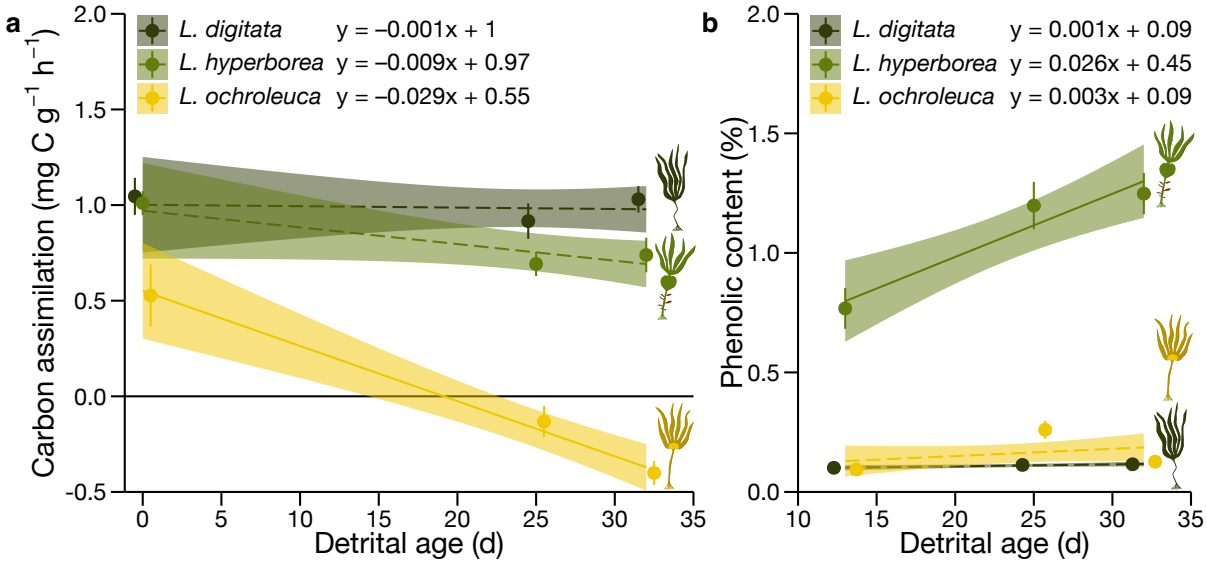

Figure 6. Consequences of decomposition for Northeast Atlantic *Laminaria* species detritus. **a**, Decomposition has a contrasting effect on the net primary production of cold temperate and warm temperate species at 50.4 µmol photons m^{-2} s^{-1}. Point ranges indicate means ± s.e.m. (n = 18, except at T_0 n = 6). Lines and shaded areas are model predictions and 95% confidence intervals. Solid lines represent significant slopes at the 95% confidence level, while dashed lines indicate no significant change over time. Carbon assimilation was calculated from oxygen production, assuming a photosynthetic quotient of 1, and is given per g of dry mass. **b**, Decomposition only increases the chemical defences of *Laminaria hyperborea*. Point ranges indicate means ± s.e.m. (n = 9). Lines and shaded areas are model predictions and 95% confidence intervals. Solid lines represent significant slopes at the 95% confidence level, while dashed lines indicate no significant change over time.

We also uncovered a potential negative feedback loop. Chemical defence compounds increase at a rate of 0.03% d^{-1} in *L. hyperborea* (cf. 0.06% d^{-1} over the first six weeks[36]) while they remained low and unchanged in the other species (Fig. 6b). Since phenolic content may decrease decomposition (Fig. 4b) and wounding causes the production of phlorotannins in *L. hyperborea*[45], an induced defence response to detritivore activity provides a tantalising explanation for this observation. Carbon content, which also decreases decomposition[12] (Fig. 4a), increases at a rate of 0.14% d^{-1} in *L. digitata* (Fig. S8a) and tends to diverge between cold and warm temperate species with detrital age. The carbon-nitrogen ratio conversely declines at an exponential rate of 0.005 d^{-1} in all species (Fig. S8b, cf. ref.[36]). In conclusion, this would mean that rather than becoming accessible to more consumers through decomposition, detritus of cold temperate kelps defends itself or becomes less palatable and therefore maintains integrity for longer. If proven to be correct, this putative negative feedback loop would also increase interspecific variation in CSP beyond our estimates (Fig. 5).

Discussion

Despite foreseeably diminishing CSP in a warmer climate, there is scope for the preservation of this regulating ecosystem service. Besides the need for reducing anthropogenic carbon emission emphasised here, kelp blue carbon function could potentially be maintained through marine protected areas[46], reforestation[47] and hybridisation[48] alongside restrictions on eutrophication and sedimentation[31,39]. The latter have the potential to be innovative alternatives for Annex I parties like the UK, US and Australia, which have few ocean-based NDCs[3]. Enhancement of macroalgal CDR, termed seaweed offsetting[49] or ocean afforestation[50], is currently heatedly debated on a weak empirical foundation. Both proponents[49] and opponents[50] are making high-level claims on the basis of extrapolation from single, fundamentally different macroalgal genera (*Macrocystis*[49] and *Sargassum*[50]). Here we show that in truth interspecific diversity in CSP is substantial within a single macroalgal genus, rendering this debate inutile without further empirical evidence.

Developing accuarte estimates of macroalgal contribution to global carbon sequestration will need a more nuanced understanding of different factors causing variability. Therefore, important future research goals are (1) quantifying the effect of forest state and composition on regional carbon burial, (2) measuring variance in decomposition speed between additional species and across depth and (3) unravelling microbial and macrofaunal detrital pathways in the shallow and deep ocean (Fig. S9). To achieve these goals and understand how climate change is affecting marine ecosystem

services more broadly, we argue that interspecific diversity should always be considered and more multidisciplinary research is required to bridge the void between disconnected scientific branches. Specifically, interdisciplinary links between physiology, ecology, biogeography, biogeochemistry, physics and genetics are now needed more than ever to understand the function of marine plants in a rapidly changing environment.

Data and code availability

All datasets and annotated R scripts written for this study are available in the open-access repository at github.com/lukaseamus/CSP. We place no restrictions on data and code availability. L.S.W. maintains the repository and may be contacted for further requests.

Acknowledgements

We express our gratitude to the University of Plymouth technicians Marie Palmer, Jane Akerman, Richard Ticehurst, Andy Atfield and Billy Simmonds. Special thanks go to Richard Billington for his assistance with the colorimetric assay. We would also like to thank Nadia Frontier, Isla MacMillan, Harry Teagle, Graham Epstein, Martina Mulas, Dan Smale and the dive team at the University of Plymouth for assistance with fieldwork and sample processing. Moreover, L.S.W. received valuable information through correspondence with Just Cebrián, Ana de Moura Queirós, María Jesús García-Sánchez, João Nuno Franco, Florian de Bettignies, Kai Bischof and Klaus Lüning.

Author contributions

L.S.W. and A.F. designed the study and collected data on decomposition, phenolic content, elemental stoichiometry and photosynthesis. A.P. collected data on decomposition, standing stock and carbon export. L.S.W. analysed and visualised all data and performed all modelling and estimation. L.S.W. wrote the draft version of the manuscript. All authors edited and approved the final manuscript.

Competing interests

The authors declare no competing interests.

References

1. Canadell, J. G. et al. in *Climate Change 2021: The Physical Science Basis. Contribution of Working Group I to the Sixth Assessment Report of the Intergovernmental Panel on Climate Change* (eds Masson-Delmotte, V. et al.) (Cambridge University Press, Cambridge, 2021).
2. Smith, S. V. Marine macrophytes as a global carbon sink. *Science* **211**, 838–840 (1981).
3. Gallo, N. D., Victor, D. G. & Levin, L. A. Ocean commitments under the Paris Agreement. *Nat. Clim. Chang.* **7**, 833–838 (2017).
4. Bertram, C. et al. The blue carbon wealth of nations. *Nat. Clim. Chang.* **11**, 704–709 (2021).
5. Krause-Jensen, D. et al. Sequestration of macroalgal carbon: the elephant in the blue carbon room. *Biol. Lett.* **14**, 20180236 (2018).
6. Duarte, C. M. & Cebrián, J. The fate of marine autotrophic production. *Limnol. Oceanogr.* **41**, 1758–1766 (1996).
7. Cebrián, J., Duarte, C. M., Marbà, N. & Enríquez, S. Magnitude and fate of the production of four co-occurring Western Mediterranean seagrass species. *Mar. Ecol. Prog. Ser.* **155**, 29–44 (1997).
8. Pessarrodona, A., Foggo, A. & Smale, D. A. Can ecosystem functioning be maintained despite climate-driven shifts in species composition? Insights from novel marine forests. *J. Ecol.* **107**, 91–104 (2019).
9. Pessarrodona, A., Moore, P. J., Sayer, M. D. J. & Smale, D. A. Carbon assimilation and transfer through kelp forests in the NE Atlantic is diminished under a warmer ocean climate. *Glob. Chang. Biol.* **24**, 4386–4398 (2018).
10. Pedersen, M. F. et al. Detrital carbon production and export in high latitude kelp forests. *Oecologia* **192**, 227–239 (2020).
11. Enríquez, S., Duarte, C. M. & Sand-Jensen, K. Patterns in decomposition rates among photosynthetic organisms: the importance of detritus C:N:P content. *Oecologia* **94**, 457–471 (1993).
12. Filbee-Dexter, K. et al. Ocean temperature controls kelp decomposition and carbon sink potential. Preprint at http://dx.doi.org/10.21203/rs.3.rs–38503/v1 (2020).

13. Cebrián, J. & Duarte, C. M. Plant growth-rate dependence of detrital carbon storage in ecosystems. *Science* **268**, 1606–1608 (1995).
14. Trevathan-Tackett, S. M. et al. Comparison of marine macrophytes for their contributions to blue carbon sequestration. *Ecology* **96**, 3043–3057 (2015).
15. Amsler, C. D. *Algal chemical ecology* (Springer, Berlin, 2008).
16. Duarte, C. M., Losada, I. J., Hendriks, I. E., Mazarrasa, I. & Marbà, N. The role of coastal plant communities for climate change mitigation and adaptation. *Nat. Clim. Chang.* **3**, 961–968 (2013).
17. Krause-Jensen, D. & Duarte, C. M. Substantial role of macroalgae in marine carbon sequestration. *Nat. Geosci.* **9**, 737–742 (2016).
18. Queirós, A. M. et al. Connected macroalgal-sediment systems: blue carbon and food webs in the deep coastal ocean. *Ecol. Monogr.* **89**, e01366 (2019).
19. Lavery, P. S., Mateo, M. Á., Serrano, O. & Rozaimi, M. Variability in the carbon storage of seagrass habitats and its implications for global estimates of blue carbon ecosystem service. *PLoS One* **8**, e73748 (2013).
20. Atwood, T. B. et al. Global patterns in mangrove soil carbon stocks and losses. *Nat. Clim. Chang.* **7**, 523–528 (2017).
21. Li, S. et al. Factors regulating carbon sinks in mangrove ecosystems. *Glob. Chang. Biol.* **24**, 4195–4210 (2018).
22. Wernberg, T. & Filbee-Dexter, K. Grazers extend blue carbon transfer by slowing sinking speeds of kelp detritus. *Sci. Rep.* **8**, 17180 (2018).
23. Filbee-Dexter, K., Wernberg, T., Norderhaug, K. M., Ramirez-Llodra, E. & Pedersen, M. F. Movement of pulsed resource subsidies from kelp forests to deep fjords. *Oecologia* **187**, 291–304 (2018).
24. Tala, F. et al. Long-term persistence of the floating bull kelp *Durvillaea antarctica* from the South-East Pacific: potential contribution to local and transoceanic connectivity. *Mar. Environ. Res.* **149**, 67–79 (2019).
25. Fraser, C. I. et al. Antarctica's ecological isolation will be broken by storm-driven dispersal and warming. *Nat. Clim. Chang.* **8**, 704–708 (2018).
26. Filbee-Dexter, K. & Wernberg, T. Substantial blue carbon in overlooked Australian kelp forests. *Sci. Rep.* **10**, 12341 (2020).
27. Smale, D. A., Wernberg, T., Yunnie, A. L. E. & Vance, T. The rise of *Laminaria ochroleuca* in the Western English Channel (UK) and comparisons with its competitor and assemblage dominant *Laminaria hyperborea*. *Mar. Ecol.* **36**, 1033–1044 (2015).
28. Parke, M. *Laminaria ochroleuca* de la Pylaie growing on the coast of Britain. *Nature* **162**, 295–296 (1948).
29. Lüning, K. *Seaweeds: their environment, biogeography, and ecophysiology* (John Wiley & Sons, Inc., Hoboken, 1990).
30. Abdullah, M. I. & Fredriksen, S. Production, respiration and exudation of dissolved organic matter by the kelp *Laminaria hyperborea* along the west coast of Norway. *J. Mar. Biol. Assoc. U.K.* **84**, 887–894 (2004).
31. Blain, C. O., Hansen, S. C. & Shears, N. T. Coastal darkening substantially limits the contribution of kelp to coastal carbon cycles. *Glob. Chang. Biol.* 10.1111/gcb.15837 (2021).
32. Hereward, H. F. R., Foggo, A., Hinckley, S. L., Greenwood, J. & Smale, D. A. Seasonal variability in the population structure of a habitat-forming kelp and a conspicuous gastropod grazer: do blue-rayed limpets (*Patella pellucida*) exert top-down pressure on *Laminaria digitata* populations? *J. Exp. Mar. Biol. Ecol.* **506**, 171–181 (2018).
33. de Bettignies, F. et al. Temporal succession of a macrofaunal community associated with kelp fragment accumulations in an *in situ* experiment. *Mar. Ecol. Prog. Ser.* **656**, 109–121 (2020).
34. Hargrave, M. S., Foggo, A., Pessarrodona, A. & Smale, D. A. The effects of warming on the ecophysiology of two co-existing kelp species with contrasting distributions. *Oecologia* **183**, 531–543 (2017).
35. Cosse, A., Potin, P. & Leblanc, C. Patterns of gene expression induced by oligoguluronates reveal conserved and environment-specific molecular defense responses in the brown alga *Laminaria digitata*. *New Phytol.* **182**, 239–250 (2009).

36. de Bettignies, F. et al. Degradation dynamics and processes associated with the accumulation of *Laminaria hyperborea* (Phaeophyceae) kelp fragments: an in situ experimental approach. *J. Phycol.* **56**, 1481–1492 (2020).
37. Smale, D. A. Impacts of ocean warming on kelp forest ecosystems. *New Phytol.* **225**, 1447–1454 (2020).
38. Krumhansl, K. A., Lauzon-Guay, J.-S. & Scheibling, R. E. Modeling effects of climate change and phase shifts on detrital production of a kelp bed. *Ecology* **95**, 763–774 (2014).
39. Pessarrodona, A. et al. Homogenization and miniaturization of habitat structure in temperate marine forests. *Glob. Chang. Biol.* **27**, 5262–5275 (2021).
40. Smale, D. A. et al. Marine heatwaves threaten global biodiversity and the provision of ecosystem services. *Nat. Clim. Chang.* **9**, 306–312 (2019).
41. King, N. G. et al. Ecological performance differs between range centre and trailing edge populations of a cold-water kelp: implications for estimating net primary productivity. *Mar. Biol.* **167**, (2020).
42. Pedersen, M. F., Filbee-Dexter, K., Frisk, N. L., Sárossy, Z. & Wernberg, T. Carbon sequestration potential increased by incomplete anaerobic decomposition of kelp detritus. *Mar. Ecol. Prog. Ser.* **660**, 53–67 (2021).
43. Frontier, N., de Bettignies, F., Foggo, A. & Davoult, D. Sustained productivity and respiration of degrading kelp detritus in the shallow benthos: detached or broken, but not dead. *Mar. Environ. Res.* **166**, 105277 (2021).
44. Wright, L. S. & Foggo, A. Photosynthetic pigments of co-occurring Northeast Atlantic *Laminaria* spp. are unaffected by decomposition. *Mar. Ecol. Prog. Ser.* 10.3354/meps13886 (2021).
45. Halm, H., Lüder, U. H. & Wiencke, C. Induction of phlorotannins through mechanical wounding and radiation conditions in the brown macroalga *Laminaria hyperborea*. *Eur. J. Phycol.* **46**, 16–26 (2011).
46. Ling, S. D., Johnson, C. R., Frusher, S. D. & Ridgway, K. R. Overfishing reduces resilience of kelp beds to climate-driven catastrophic phase shift. *Proc. Natl. Acad. Sci. U.S.A.* **106**, 22341–22345 (2009).
47. Layton, C. et al. Kelp forest restoration in Australia. *Front. Mar. Sci.* **7**, 74 (2020).
48. Martins, N. et al. Hybrid vigour for thermal tolerance in hybrids between the allopatric kelps *Laminaria digitata* and *L. pallida* (Laminariales, Phaeophyceae) with contrasting thermal affinities. *Eur. J. Phycol.* **54**, 548–561 (2019).
49. Froehlich, H. E., Afflerbach, J. C., Frazier, M. & Halpern, B. S. Blue growth potential to mitigate climate change through seaweed offsetting. *Curr. Biol.* **29**, 3087–3093 (2019).
50. Bach, L. T. et al. Testing the climate intervention potential of ocean afforestation using the Great Atlantic Sargassum Belt. *Nat. Commun.* **12**, 2556 (2021).

Methods

1. Empirical data

1.1 Sporophyte density

The sporophyte density of each *Laminaria* species at West Hoe (50.363629°N, 4.144978°W) in Plymouth Sound (UK) was measured between January 2016 and March 2017 by haphazardly placing 1-m^2 quadrats in the lower eulittoral zone (*L. digitata*) and upper infralittoral zone (*L. hyperborea* and *L. ochroleuca*) during low spring tides and counting mature plants.

1.2 Carbon export

To measure species-specific carbon export, we quantified the release of detritus via distal lamina erosion[1,2] at West Hoe (50.363629°N, 4.144978°W) between March 2016 and February 2017. We used erosion as a conservative measure of the total carbon exported from kelp forests, which also includes carbon exported as entire dislodged plants[2–4] as well as carbon exported in dissolved form[5,6]. Each month, ten plants of each species were tagged and uniquely labelled during low spring tides. Three holes were punched in every sporophyte, two at 10 and 15 cm above the stipe-lamina connection on the central digit, and another one at 15 cm above the stipe-lamina connection on an outer digit. This initial hole position (H_I) and the initial length of each punched digit (L_I) were recorded. After a month, tagged plants were collected and returned to the laboratory, where the final digit lengths (L_F) and final hole positions (H_F) for each plant were measured. The lamina length loss for

each plant (M, cm plant^{-1} mo^{-1}) was calculated by averaging the tissue loss from the central ($_1$) and outer ($_2$) digits as

$$M = \frac{L_{1I} + G_1 - L_{1F} + L_{2I} + G_2 - L_{2F}}{2}$$

where G, the length growth of each digit (cm mo^{-1}), is $H_F - H_I$. To convert the loss of tissue length (cm) to biomass (g), three 5-cm segments from the most distal part of each retrieved lamina were cut and their wet mass recorded. We determined the relationship between wet and dry mass by drying the outermost segment at 60°C for 48 h. Wet mass consistently correlated well with dry mass ($R^2 \geq 0.89$). We then estimated the dry mass of the rest of the 5-cm segments for each plant using this wet to dry mass ratio. Dry mass per unit length was then averaged between the three segments to give the distal lamina dry mass to length ratio (g cm^{-1}). The daily erosion rate (E, g plant^{-1} d^{-1}) was calculated as

$$E = \frac{M \times ML_R}{\Delta t}$$

where M is lamina length loss (cm plant^{-1} mo^{-1}), ML_R is the dry mass to length ratio (g cm^{-1}) and Δt is the number of elapsed days (d mo^{-1}). Finally, these biomass erosion rates were converted to carbon export (g C plant^{-1} d^{-1}) using a site-and species-specific carbon content (%) obtained from sampling three mature sporophytes approximately every two months. Kelp tissue from each sampled individual was lyophilised (Lablyo, Frozen in Time Ltd, York, UK), ground and its carbon content quantified using an elemental analyser (CHN analyser, EA1110, CE Instruments Ltd, Wigan, UK).

1.3 Decomposition

In situ decomposition rates were derived from two independently run field mesh bag experiments conducted in Plymouth Sound, UK in 2016 and 2019 respectively. In 2016, lamina material from each *Laminaria* species was collected in March and cut into ~5 × 15-cm strips. A total of 105 ± 8 g of fresh kelp strips was then sealed within eight mesh bags (2- and 20-mm mesh ø) per species, which were then deployed at 4 m below lowest astronomical tide on a sandy seabed adjacent to kelp forests at Drake's Island (50.353328°N, 4.150224°W) and Jennycliff (50.343059°N, 4.131762°W). Litter bags were attached to a long rope, positioned ca. 1 m apart from one another, and secured to the seabed with anchor weights. Upon retrieval after 40–41 d, a fine mesh bag (1-µm ø) was placed over each litter bag to retain all kelp material and detritivores, before detaching the bag from the rope. In the laboratory, the contents of the bags were carefully removed and washed through a 1-mm sieve. Remaining kelp tissue was weighed.

In 2019, nine mature sporophytes of each species were collected at West Hoe (50.363629°N, 4.144978°W) on 17th May and four fronds removed from each *in situ*. The first of these was placed in a cooler for transport to the laboratory, while the other three were trimmed to weigh 20 ± 1 g. Frond samples were taken from the central part of the current year's lamina growth, avoiding the meristematic basal and eroding distal regions. For each species, one frond sample from each sporophyte was placed within each of three rectangular, galvanised steel mesh enclosures (62.4 × 34.4 cm, 13-mm mesh ø). The nine mesh cages were then chained together, closed with cable ties and deployed at 2 m below lowest astronomical tide within the kelp forest at West Hoe. A temperature and light logger (HOBO Pendant®, Onset, Massachusetts, USA) was secured to one end of the chain facing the surface and the chain was deployed parallel to the shoreline to control for depth. Samples were retrieved on 30th May, 11th June and 18th June (i.e. after 13, 25 and 32 d). On each retrieval date, three randomly selected frond samples were removed from each litter bag and weighed using an analytical balance (± 1 mg, Fisherbrand™ Precision Series, Fisher Scientific, Loughborough, UK). Decomposition (D, % d^{-1}) was calculated as

$$D = \frac{(M_0 - M_1) \times 100}{M_0 \times \Delta t}$$

where M_0 is the initial sample mass (20 ± 1 g), M_1 is the retrieved sample mass (g) and Δt is the time period (d). Two subsamples (1.5–2 g) were then refrigerated at ~3°C to retain cellular function for subsequent photophysiological measurements, while the rest of the sample was frozen at –20°C for elemental and phenolic analyses.

1.4 Primary production and respiration

Gross primary production (GPP) is true photosynthesis minus photorespiration, while net primary production (NPP) further accounts for respiration (R)[7]. According to the definition used here, NPP attains negative values when photosynthetic supply cannot cover respiratory demand and stored carbon (i.e. old production) is respired in addition to new production[8].

NPP and R of refrigerated duplicate subsamples from West Hoe were measured via closed bottle respirometry within five (more often two) days of collection. These measurements were performed by quantifying light and dark oxygen (O_2) evolution in 130 ± 5-ml glass incubation jars[9]. Sample mass was recorded as buoyant rather than blotted wet mass to keep the microbial biofilm intact and then converted. Incubations were exposed to 50.4 µmol photons m^{-2} s^{-1}. This light treatment is within the saturation range for *Laminaria* species[10] and representative of a previously measured mean *Laminaria* forest photoenvironment at 2 m depth in spring (60.7 µmol photons m^{-2} s^{-1})[11]. Each set of measurements was accompanied by a 270 ± 5-ml blank incubation. All incubation jars were fitted with 5-mm diameter planar oxygen sensitive spots (PreSens, Regensburg, Germany) and magnetic stir bars (Fisherbrand™, Fisher Scientific, Loughborough, UK) and placed on a magnetic stirrer (MIX 15 eco, 2mag AG, München, Germany), set at 350 rpm. Measurements were taken with a fibre optic O_2 meter (Fibox 4 trace, PreSens, Regensburg, Germany) after 10 and 30 min in a 20°C controlled temperature room. Any fluctuation in temperature was accounted for by the O_2 meter's temperature probe, which was placed in a water bath alongside the stirrer. Seawater salinity (33–35‰) was measured prior to incubation and the O_2 meter's settings were modified accordingly. NPP (µmol O_2 g^{-1} min^{-1}), R (µmol O_2 g^{-1} min^{-1}) and GPP (µmol O_2 g^{-1} min^{-1}) were subsequently calculated as

$$NPP = \frac{(c_{S_1} - c_{S_0}) \div V_S - (c_{B_1} - c_{B_0}) \div V_B}{M \times \Delta t}$$

$$R = \frac{(c_{S_0} - c_{S_1}) \div V_S - (c_{B_0} - c_{B_1}) \div V_B}{M \times \Delta t}$$

$$GPP = NPP + R$$

where c is the molar O_2 concentration (µmol O_2 l^{-1}), V is the incubation volume (l), M is the sample wet mass (g) and Δt is the time window (min). $_S$ refers to incubations containing a sample, while $_B$ refers to blank incubations. Subscript numbers represent the time of measurement. All values were averaged across the 10- and 20-min incubation periods for each sample and converted to µmol O_2 g^{-1} h^{-1}. Net carbon assimilation (CA) per g of dry mass (g C g^{-1} h^{-1}) was then calculated from NPP (µmol O_2 g^{-1} h^{-1}) as

$$CA = \frac{NPP \times 10^{-6} \times 12.0107}{M_R}$$

where 10^{-6} is the conversion factor from µmol to mol, 12.0107 is the atomic mass of C and M_R is the dry mass to wet mass ratio measured at West Hoe in May 2016. Gross CA was calculated from GPP in the same way. This calculation assumes a photosynthetic quotient (PQ) and respiratory quotient of 1. We are aware that in reality PQ changes with depth[12] and light exposure[13] in *Laminaria hyperborea* and varies interspecifically in brown algae[14]. However, an extensive literature search and correspondence with various European phycologists revealed no usable PQs for interspecific comparison.

On the first day of sample retrieval (30th May), air temperature (22.9°C) and photon fluence rate (2618 µmol photons m^{-2} s^{-1}) were extremely high. At 971 µmol photons m^{-2} s^{-1}, well below the observed irradiance on that day, photoinhibition was previously shown to reduce *in situ* O_2 production of *L.*

digitata[15]. After photoinhibition was confirmed during the data exploration stage, primary production and respiration data from this day were removed from the statistical analysis.

1.5 Elemental stoichiometry

Frozen subsamples were lyophilised (Lablyo, Frozen in Time Ltd, York, UK) and subsequently ground to 250-µm powder. Powder samples of ~2 mg (± 0.01 mg, AT201, Mettler Toledo, Leicester, UK) were then sealed in 6 × 4-mm tin capsules (OEA Laboratories Ltd, Exeter, UK) and combusted in an elemental analyser CHN analyser, EA1110, CE Instruments Ltd, Wigan, UK) to measure their C and nitrogen (N) content (%). Acetanilide (C_8H_9NO, OEA Laboratories Ltd, Exeter, UK) was chosen as the analytical standard because of its high C (71.09%) and low N (10.36%) content.

1.6 Phenolic content

Total polyphenolic content was measured using a high-throughput 96-well microplate Folin-Ciocalteu colorimetric assay[16]. 50 mg of ground, freeze-dried kelp was added to 500 µl of 100% methanol and vortexed (Whirlimixer, Fisons, Ipswich, UK) for ~10 s in a 1.5-ml microtube. The solute was left to be extracted for one hour, after which the 10% (w/v) solution was vortexed again and then centrifuged at 14000 × *g* for 5 min. The supernatant was transferred into another microtube and immediately stored at –20°C. Phloroglucinol (PG) (Sigma-Aldrich, Gillingham, UK), used as the phenol standard, was dissolved in 100% methanol at concentrations of 0.05, 0.1, 0.25, 0.5, 0.75 and 0.1 mg ml^{-1}. In a 96-well microplate, 10 µl of each PG solution was added to 100 µl of 10% (diluted with distilled water) Folin-Ciocalteu reagent (Sigma-Aldrich, Gillingham, UK) and, after a 5-min reaction period, 90 µl of 1 M Na_2CO_3 solution was added last. To produce the standard curve, absorbance of each PG concentration was measured at 765 nm using a microplate reader (FLUOstar® Omega, BMG Labtech Ltd, Aylesbury, UK). After centrifugation at 14000 × *g* for 1 min to eliminate remaining particulates, sample extracts were prepared and their absorbance recorded as described above. All measurements were taken in triplicates and with solvent blanks. Using the derived standard curve equation y = 1.91 x – 0.07, phenolic content (P, %) was calculated in PG equivalents as

$$P = \frac{A + 0.07}{1.91}$$

where A is sample extract absorbance (arbitrary units).

1.7 Grazing pressure

Grazing impact by macrodetritivores such as *Steromphala cineraria*[1,16–18] and *Patella pellucida*[1,16–19] was estimated by measuring the area of excavation and perforation scars via image analysis[19] after the 2019 decomposition experiment. Excavation here refers to a paling of the lamina surface that is associated with excavation by algivorous gastropods[20] but may also be caused by saprotrophic microbes. Perforations are defined as holes in the lamina that are most likely caused by gastropod radulae during prolonged grazing[20]. Samples, retrieved after 32 d (18th June), were photographed next to a ruler (± 1 mm) under identical lighting. Images were then analysed with Fiji (ImageJ v2.0.0-rc-69/1.52p)[21]. The surface areas of holes and discoloured tissue were measured manually, while total surface area was measured by making the image binary and highlighting the sample edges. The areas of excavation (E, %) and perforation (P, %) were calculated as

$$E = \frac{A_E \times 100}{A_T - A_P}$$

$$P = \frac{A_P \times 100}{A_T}$$

where A_E is the excavated area, A_T is the total area and A_P is the perforated area.

2. Estimation

2.1 Present areal carbon export and carbon sequestration potential

Species-specific carbon sequestration potential (CSP) was estimated using empirical sporophyte density, carbon export and decomposition data (methods sections 1.1–1.3). The CSP estimation was

carried out in R v4.0.2[22] within the integrated development environment RStudio v1.3.1093[23] and can be accessed at github.com/lukaseamus/CSP/Sequestration.

The kelp forest at West Hoe forms a ~20-m band, the upper ~4 m of which are occupied only by *Laminaria digitata*, while the lower ~16 m consist of a mixed stand of *L. hyperborea* and *L. ochroleuca* (L.S. Wright, personal observation). To account for this vertical distribution, sporophyte density (plants m^{-2}) for each species was multiplied by the relative space it occupies in the kelp forest (0.2 in the case of *L. digitata* and 0.8 in the case of *L. hyperborea* and *L. ochroleuca*). Seasonal and annual carbon export were obtained by multiplying daily carbon export (g C $plant^{-1}$ d^{-1}) for each month by the number of days in that month, then calculating the mean monthly carbon export and finally summing those means across season or year. According to the variance sum law, standard errors of the annual means (SE_S) were estimated as

$$SE_S = \sqrt{SE_1^2 + SE_2^2 + \ldots + SE_{12}^2}$$

where $SE_{1–12}$ are the standard errors of individual months. See github.com/lukaseamus/CSP/Export for details. Decomposition rates (D, % d^{-1}), which were measured in spring and early summer (methods section 1.3), were converted to proportional temperature-corrected decomposition rates (D_C, proportion d^{-1}) as

$$D_C = \frac{D + 0.051 \times (T - T_E)}{100}$$

where 0.051 is the slope of the positive relationship between *L. hyperborea* and *Saccharina latissima* decomposition (% d^{-1}) and temperature (°C)[24], T is the annual or seasonal mean temperature (°C) and T_E is the mean *in situ* experimental temperature (°C) during the decomposition period, measured with a temperature and light logger (HOBO Pendant®, Onset, Massachusetts, USA). Finally, the change in present seasonal and annual CSP (g C m^{-2} $season^{-1}$ or g C m^{-2} yr^{-1}) with detrital age was estimated for each species as

$$CSP = N \times CE \times (1 - t \times D_C)$$

where N is the seasonal or annual mean number of sporophytes (plants m^{-2}), CE is the seasonal or annual carbon export (g C $plant^{-1}$ $season^{-1}$ or g C $plant^{-1}$ yr^{-1}), t is the detrital age (d) and D_C is the temperature-corrected decomposition rate (proportion d^{-1}). According to the rules of estimating variance around the product of two means[25], the seasonal and annual 95% confidence intervals (CI) around CSP were estimated for each species as

$$CI = CSP \pm z \times \sqrt{SE_N^2 \times SE_{CE}^2 + SE_N^2 \times \overline{X}_{CE}^2 + SE_{CE}^2 \times \overline{X}_N^2}$$

where z is the 97.5 percentile point of the standard normal distribution, $\overline{X}_N$ and SE_N are the seasonal or annual means and standard errors of sporophyte density (plants m^{-2}) and $\overline{X}_{CE}$ and SE_{CE} are the seasonal or annual means and standard errors of carbon export (g C $plant^{-1}$ $season^{-1}$ or g C $plant^{-1}$ yr^{-1}). The same equation was used to estimate 95% confidence intervals around estimates of annual areal carbon export (g C m^{-2} yr^{-1}).

2.2 Areal carbon export and carbon sequestration potential through time

To test the effect of past and future ocean temperature on CSP, sporophyte densities were modelled according to species-specific temperature tolerances (Fig. 2b, Table S4), historical sea surface temperature data at 1° spatial resolution[26] and representative concentration pathway (RCP) temperature predictions at 5-arcmin spatial resolution[27] for the region around West Hoe (50.363629°N, 4.144978°W). Minimum (February), mean and maximum (August) temperature data were extracted from both datasets with the R package raster v3.4-5[28] and a trendline was fit using locally estimated scatterplot smoothing (polynomial regression) with smoothing parameter α = 1 (Fig. S4).

In the region of latitudinal range overlap (Fig. 2a), warm temperate *Laminaria ochroleuca* is currently limited by minimum temperatures while cold temperate *L. digitata* and *L. hyperborea* are limited by maximum temperatures[29]. Moreover, it is likely that the limiting factor at the leading range edge is gametophyte fertility: gametophytes, the prerequisite for sporophytes[10], are the first to arrive in a new locality. This is supported by the arrival of *L. ochroleuca* in Plymouth Sound in 1946[30], when maximum sea surface temperatures were approximately 9.53°C, close to the lowest tolerance of 10°C for gametophyte fertility (Table S4). Conversely, trailing edge populations are likely limited by sporophyte growth: due to their perennial nature[10] *Laminaria* sporophytes may hang on for several years after temperatures become suboptimal for reproduction. This is evidenced by the slower retraction of trailing edge populations of benthic macroalgae than their leading edge populations expand[31]. Therefore, using the estimated maximum (T_{max}) and minimum (T_{min}) temperature trends, plant densities for cold temperate (N_C) and warm temperate (N_W) species were modelled through time as

$$N_C = \frac{N \times (T_U - T_{max})}{(T_U - T_{max2016})}$$

$$N_W = \frac{N \times (T_{min} - T_L)}{(T_{min2016} - T_L)}$$

where N is the mean number of plants (m^{-2}) in 2016 (methods section 1.1), T_U is the upper temperature limit (i.e. temperature just outside the tolerance range) for cold temperate sporophyte growth, T_L is the lower temperature limit for warm temperate gametophyte fertility (note that this was adjusted from 10°C to approximately 9.53°C because *L. ochroleuca* can establish a population at this sea surface temperature[30]), $T_{min2016}$ and $T_{max2016}$ are the minimum and maximum sea surface temperatures for 2016, the year for which plant density measurements are available (methods section 1.1).

Importantly, *L. ochroleuca* cannot occupy the vertical zone of *L. digitata* because it cannot tolerate emersion[32]. Therefore, the plant density of this warm temperate species was limited to the total observed sporophyte density (*L. hyperborea* + *L. ochroleuca*) in the lower ~16-m band of the kelp forest in 2016. Using the modelled plant densities (N_M, m^{-2}), long-term trends in annual carbon export (CE_T, g C m^{-2} yr^{-1}) and CSP (CSP_T, g C m^{-2} yr^{-1}) were estimated as

$$CE_T = N_M \times CE$$

$$CSP_T = N_M \times CE \times (1 - t \times \frac{D + 0.051 \times (T_{\bar{X}} - T_E)}{100})$$

where CE is annual carbon export (g C $plant^{-1}$ yr^{-1}), t is the detrital age (d) at which sequestration is assumed (the example provided uses t = 50 d to illustrate a scenario where all species would contribute to overall CSP), D is decomposition (% d^{-1}), 0.051 is the slope of the positive relationship between *L. hyperborea* and *Saccharina latissima* decomposition (% d^{-1}) and temperature (°C)[24], $T_{\bar{X}}$ is the estimated mean temperature trend and T_E is the mean *in situ* experimental temperature (°C) during the decomposition period, measured with a temperature and light logger (HOBO Pendant®, Onset, Massachusetts, USA).

Trends in annual CE and CSP for the entire *Laminaria* forest were derived by summing CE_T and CSP_T across species. The variance sum law was again applied to estimate 95% confidence intervals (methods section 2.1). To illustrate the difference in magnitude between climate-driven CSP decline due to accelerated decomposition on its own[24] and in combination with the shifts in kelp forest composition we model here, N_M was alternatively kept at the 2016 level in the above equations.

2.3 Cumulative detrital carbon assimilation potential

Detritus of *Laminaria* species maintains primary production for months[33,34]. However, it also sinks immediately due to lack of pneumatocysts or porous tissue, as was previously observed for *L. hyperborea*[35]. Nonetheless, kelp detritus may assimilate significant amounts of carbon while resting on shallow seabed as evidenced by the growth of some *Laminaria* detritus[33,34,36]. The reason may be

periodically high photon flux densities (e.g. 142.7 µmol photons m^{-2} s^{-1} at 2 m depth in July)[11] that cause photosynthesis to mask decomposition. During our *in situ* decomposition experiment (methods section 1.3), light was very limited due to shading by the kelp canopy and turbidity (daytime mean = 0.54 µmol photons m^{-2} s^{-1}, overall mean = 0.36 µmol photons m^{-2} s^{-1}). This invited an exploration of how our detritus might have assimilated carbon had there been different photon flux densities.

To estimate how net carbon assimilation may change throughout the detrital phase, we made use of our empirical gross carbon assimilation data (methods section 1.4), the mentioned low light regime during the decomposition experiment, seasonal and annual average daylight hours for the Plymouth Sound region, depth profiles of photosynthetically active radiation (PAR) for the Plymouth Sound region between 2009 and 2020[37], the photosynthesis-irradiance relationship for *Laminaria hyperborea*[38] along with the location and depth of the local kelp carbon sink[39]. Because respiration is assumed to stay constant under changing light (GPP is calculated as NPP + R on these grounds), we were able to estimate the potential for detrital net carbon assimilation under various light regimes.

First, the seasonal and annual excess (in a brighter photoenvironment) gross carbon assimilation as a proportion of laboratory GPP needs to be determined. In the following equation the term left of the multiplication sign calculates the proportion of laboratory GPP that remains after accounting for *in situ* GPP during our decomposition experiment. The right term signifies the proportion of laboratory GPP at various stages in the detrital phase. When multiplied, the terms thus yield a function that gives the proportion by which laboratory GPP must be adjusted (P_{GPP}):

$$P_{GPP} = \left(1 - \frac{PI(PAR_F)}{PI(PAR_L)}\right) \times \frac{PI(PAR_D(t \times v \div \sqrt{m^2 + 1} \times m))}{PI(PAR_L)}$$

where PI is the photosynthesis-irradiance function $y = 1.8 \times tanh(\frac{0.006x}{1.8})$, PAR_F and PAR_L are the mean daytime photon flux density during the field experiment (0.54 µmol photons m^{-2} s^{-1}) and the laboratory irradiance (50.4 µmol photons m^{-2} s^{-1}), PAR_D is an exponential decay function of seasonal or annual light attenuation with depth (e.g. the annual equation is $y = e^{-0.15x + 5.05}$), t is the detrital age (d), v is the minimal detrital velocity (m d^{-1}), estimated by trigonometry from the depth of the local carbon sink and its distance from the nearest kelp forest, assuming a detrital travel time of 50 d (cf. methods section 2.2), and m is the seabed slope, estimated by dividing the depth of the local carbon sink by its distance from the West Hoe kelp forest.

Second, the change in seasonal and annual cumulative net carbon assimilation (CA, g C m^{-2} $season^{-1}$ or g C m^{-2} yr^{-1}) with detrital age were estimated as

$$CA = \sum_{k=1}^{t} N \times BE \times D_{CA}(k) \times h \times GPP(k) \times P_{GPP}(k)$$

where t is the detrital age (d), N is the seasonal or annual sporophyte density (plants m^{-2}), BE is the seasonal or annual dry biomass export (g $plant^{-1}$ $season^{-1}$ or g $plant^{-1}$ yr^{-1}), D_{CA} is a special case of $1 - t \times D_C$ where $D_{CA} \geq 0$ (cf. methods section 2.1), h is the seasonal or annual daylight time (h) and GPP is the species-specific gross carbon assimilation (g C g^{-1} h^{-1}). Note that this estimate of detrital CA is conservative, since it assumes that excess production in the new light milieu cannot photosynthesise: $N \times BE \times D_{CA}(k)$ always gives the remaining biomass at each *k* irrespective of elevated production. As such CA is the carbon pool that a shrinking amount of detritus can produce as it travels to the sink. The 95% confidence intervals for CA are the same as those of the other estimates (methods section 2.1).

3. Data analysis and visualisation

Data analysis and visualisation were performed in R v4.0.2[22] within the integrated development environment RStudio v1.3.1093[23]. The output of all analyses is listed in Table S6.

Prior to analysis, data were explored using standard visualisation techniques[40]. For three response variables, all assumptions were met and standard linear models were built (Table S6). If the data distribution violated the assumption of normality, alternative distributions were explored with fitdistrplus v1.1-3[41]. In four cases, a gamma generalised linear model with a logarithmic link function fit the data best (Table S6). In the case that the assumption of homogeneity was not met, variance was modelled as a function of explanatory variables[40] with generalised least squares in nlme v3.1-151[42]. This model type fit the data best in six cases (Table S6). For every response variable, the potential influence of individual mesh bags was checked by building linear mixed effects models in nlme v3.1-151[42] or lme4 v1.1-26[43] with mesh bag identity as a random intercept and slope. These models were then tested against fixed effects models and in a single case mesh bag identity was determined to have an effect on the response variable (Table S6). Type II or III omnibus hypothesis tests were performed with car v3.0-10[44].

The package ggplot2 v3.3.3[45] was used for all data visualisation. In one specific case, monthly variation in daily carbon export, ggplot2 was augmented with the x-spline add-on geometry supplied by ggalt v0.4.0[46]. Descriptive statistics were calculated using psych v2.0.12[47]. For each different model, 95% confidence intervals were calculated as mean $\pm z \times$ s.e.m. according to ref.[48]. Plots were aligned and juxtaposed in cowplot v1.1.1[49]. The base map of Europe used in Fig. 2a was plotted with rworldmap v1.3-6[50]. Illustration and editing were performed in Affinity Designer v1.7.3 (Serif Ltd, West Bridgford, UK). The complete data analysis and visualisation pipeline can be downloaded from the open-access repository at github.com/lukaseamus/CSP.

References

1. Pessarrodona, A., Foggo, A. & Smale, D. A. Can ecosystem functioning be maintained despite climate-driven shifts in species composition? Insights from novel marine forests. *J. Ecol.* **107**, 91–104 (2019).
2. Pessarrodona, A., Moore, P. J., Sayer, M. D. J. & Smale, D. A. Carbon assimilation and transfer through kelp forests in the NE Atlantic is diminished under a warmer ocean climate. *Glob. Chang. Biol.* **24**, 4386–4398 (2018).
3. de Bettignies, T., Wernberg, T., Lavery, P. S., Vanderklift, M. A. & Mohring, M. B. Contrasting mechanisms of dislodgement and erosion contribute to production of kelp detritus. *Limnol. Oceanogr.* **58**, 1680–1688 (2013).
4. Pedersen, M. F. et al. Detrital carbon production and export in high latitude kelp forests. *Oecologia* **192**, 227–239 (2020).
5. Abdullah, M. I. & Fredriksen, S. Production, respiration and exudation of dissolved organic matter by the kelp *Laminaria hyperborea* along the west coast of Norway. *J. Mar. Biol. Assoc. U.K.* **84**, 887–894 (2004).
6. Blain, C. O., Hansen, S. C. & Shears, N. T. Coastal darkening substantially limits the contribution of kelp to coastal carbon cycles. *Glob. Chang. Biol.* 10.1111/gcb.15837 (2021).
7. Wohlfahrt, G. & Gu, L. The many meanings of gross photosynthesis and their implication for photosynthesis research from leaf to globe. *Plant Cell Environ.* **38**, 2500–2507 (2015).
8. Roxburgh, S. H., Berry, S. L., Buckley, T. N., Barnes, B. & Roderick, M. L. What is NPP? Inconsistent accounting of respiratory fluxes in the definition of net primary production. *Funct. Ecol.* **19**, 378–382 (2005).
9. Lüning, K. Growth strategies of three *Laminaria* species (Phaeophyceae) inhabiting different depth zones in the sublittoral region of Helgoland (North Sea). *Mar. Ecol. Prog. Ser.* **1**, 195–207 (1979).
10. Bartsch, I. et al. The genus *Laminaria sensu lato*: recent insights and developments. *Eur. J. Phycol.* **43**, 1–86 (2008).
11. Lüning, K. & Dring, M. J. Continuous underwater light measurement near Helgoland (North Sea) and its significance for characteristic light limits in the sublittoral region. *Helgol. Mar. Res.* **32**, 403 (1979).
12. Miller III, H. L. & Dunton, K. H. Stable isotope (^{13}C) and O_2 micro-optode alternatives for measuring photosythesis in seaweeds. *Mar. Ecol. Prog. Ser.* **329**, 85–97 (2007).
13. Miller III, H. L., Neale, P. J. & Dunton, K. H. Biological weighting functions for UV inhibition of photosynthesis in the kelp *Laminaria hyperborea* (Phaeophyceae). *J. Phycol.* **45**, 571–584 (2009).

14. Thomas, D. N. & Wiencke, C. Photosynthesis, dark respiration and light independent carbon fixation of endemic Antarctic macroalgae. *Polar Biol.* **11**, 329–337 (1991).
15. Delebecq, G. et al. In situ photosynthetic performance of *Laminaria digitata* (Phaeophyceae) during spring tides in Northern Brittany. *Cah. Biol. Mar.* **52**, 405 (2011).
16. Hargrave, M. S., Foggo, A., Pessarrodona, A. & Smale, D. A. The effects of warming on the ecophysiology of two co-existing kelp species with contrasting distributions. *Oecologia* **183**, 531–543 (2017).
17. Smale, D. A., Wernberg, T., Yunnie, A. L. E. & Vance, T. The rise of *Laminaria ochroleuca* in the Western English Channel (UK) and comparisons with its competitor and assemblage dominant *Laminaria hyperborea*. *Mar. Ecol.* **36**, 1033–1044 (2015).
18. de Bettignies, F. et al. Temporal succession of a macrofaunal community associated with kelp fragment accumulations in an *in situ* experiment. *Mar. Ecol. Prog. Ser.* **656**, 109–121 (2020).
19. Hereward, H. F. R., Foggo, A., Hinckley, S. L., Greenwood, J. & Smale, D. A. Seasonal variability in the population structure of a habitat-forming kelp and a conspicuous gastropod grazer: do blue-rayed limpets (*Patella pellucida*) exert top-down pressure on *Laminaria digitata* populations? *J. Exp. Mar. Biol. Ecol.* **506**, 171–181 (2018).
20. Krumhansl, K. A. & Scheibling, R. E. Spatial and temporal variation in grazing damage by the gastropod *Lacuna vincta* in Nova Scotian kelp beds. *Aquat. Biol.* **13**, 163–173 (2011).
21. Schindelin, J. et al. Fiji: an open-source platform for biological-image analysis. *Nat. Methods* **9**, 676–682 (2012).
22. R Core Team. *R: a language and environment for statistical computing* (R Foundation for Statistical Computing, Vienna, 2020).
23. RStudio Team. *RStudio: integrated development environment for R* (RStudio, Inc., Boston, 2020).
24. Filbee-Dexter, K. et al. Ocean temperature controls kelp decomposition and carbon sink potential. Preprint at http://dx.doi.org/10.21203/rs.3.rs–38503/v1 (2020).
25. Buonaccorsi, J. P. & Liebhold, A. M. Statistical methods for estimating ratios and products in ecological studies. *Environ. Entomol.* **17**, 572–580 (1988).
26. Rayner, N. A. Global analyses of sea surface temperature, sea ice, and night marine air temperature since the late nineteenth century. *J. Geophys. Res.* **108**, 4407 (2003).
27. Assis, J. et al. Bio-ORACLE v2.0: extending marine data layers for bioclimatic modelling. *Glob. Ecol. Biogeogr.* **27**, 277–284 (2018).
28. Hijmans, R. J. raster: geographic data analysis and modeling. *R package* **v3.4-5**. (2020).
29. van den Hoek, C. The distribution of benthic marine algae in relation to the temperature regulation of their life histories. *Biol. J. Linn. Soc.* **18**, 81–144 (1982).
30. Parke, M. *Laminaria ochroleuca* de la Pylaie growing on the coast of Britain. *Nature* **162**, 295–296 (1948).
31. García Molinos, J., Burrows, M. T. & Poloczanska, E. S. Ocean currents modify the coupling between climate change and biogeographical shifts. *Sci. Rep.* **7**, 1332 (2017).
32. King, N. G. et al. Cumulative stress restricts niche filling potential of habitat-forming kelps in a future climate. *Funct. Ecol.* **32**, 288–299 (2018).
33. de Bettignies, F. et al. Degradation dynamics and processes associated with the accumulation of *Laminaria hyperborea* (Phaeophyceae) kelp fragments: an in situ experimental approach. *J. Phycol.* **56**, 1481–1492 (2020).
34. Frontier, N., de Bettignies, F., Foggo, A. & Davoult, D. Sustained productivity and respiration of degrading kelp detritus in the shallow benthos: detached or broken, but not dead. *Mar. Environ. Res.* **166**, 105277 (2021).
35. Wernberg, T. & Filbee-Dexter, K. Grazers extend blue carbon transfer by slowing sinking speeds of kelp detritus. *Sci. Rep.* **8**, 17180 (2018).
36. Pedersen, M. F., Filbee-Dexter, K., Frisk, N. L., Sárossy, Z. & Wernberg, T. Carbon sequestration potential increased by incomplete anaerobic decomposition of kelp detritus. *Mar. Ecol. Prog. Ser.* **660**, 53–67 (2021).
37. Western Channel Observatory. L4 in-situ data station. https://westernchannelobservatory.org.uk/l4_ctdf/index.php (2021).
38. Duarte, P., Ramos, M., Calado, G. & Jesus, B. *Laminaria hyperborea* photosynthesis-irradiance relationship measured by oxygen production and pulse-amplitude-modulated chlorophyll fluorometry. *Aquat. Biol.* **19**, 29–44 (2013).

39. Queirós, A. M. et al. Connected macroalgal-sediment systems: blue carbon and food webs in the deep coastal ocean. *Ecol. Monogr.* **89**, e01366 (2019).
40. Zuur, A., Ieno, E. N., Walker, N., Saveliev, A. A. & Smith, G. M. *Mixed effects models and extensions in ecology with R* (Springer, New York, 2009).
41. Delignette-Muller, M. L. & Dutang, C. fitdistrplus: an R package for fitting distributions. *J. Stat. Softw.* **64**, 1–34 (2015).
42. Pinheiro, J., Bates, D., DebRoy, S., Sarkar, D. & R Core Team. nlme: linear and nonlinear mixed effects models. *R package* **v3.1-151**, (2020).
43. Bates, D., Mächler, M., Bolker, B. & Walker, S. Fitting linear mixed-effects models using lme4. *J. Stat. Softw.* **67**, 1–48 (2015).
44. Fox, J. & Weisberg, S. *An R companion to applied regression* (Sage, Thousand Oaks, 2019).
45. Wickham, H. *ggplot2: elegant graphics for data analysis* (Springer, New York, 2016).
46. Rudis, B. ggalt: extra coordiante systems, geoms, statitsical transformations, scales and fonts for ggplot2. *R package* **v0.4.0**, (2017).
47. Revelle, W. psych: procedures for psychological, psychometric, and personality research. *R package* **v2.0.12**, (2020).
48. Bolker, B. GLMM FAQ. http://bbolker.github.io/mixedmodels–misc/glmmFAQ.html (2021).
49. Wilke, C. O. cowplot: streamlined plot theme and plot annotations for ggplot2. *R package* **v1.1.1**. (2020).
50. South, A. rworldmap: a new R package for mapping global data. *R J.* **3**, 35–43 (2011).

Supplementary Files

This is a list of supplementary files associated with this preprint. Click to download.

- Supplements.pdf